DOI: 10.1002/smll.200701302

Contractility-Dependent Modulation of Cell Proliferation and Adhesion by Microscale Topographical Cues

Rahul G. Thakar, Matthew G. Chown, Anuj Patel, Lily Peng, Sanjay Kumar, and Tejal A. Desai**

Engineering of cellular assembly on biomaterial scaffolds by utilizing microscale topographical cues has emerged as a powerful strategy in cardiovascular tissue engineering and regenerative medicine. However, the mechanisms through which these cues are processed to yield changes in canonical cell behaviors remain unclear. Previously, we showed that when mixtures of cardiomyocytes and fibroblasts were cultured on polydimethylsiloxane surfaces studded with microscale pillars (micropegs), fibroblast proliferation was dramatically suppressed, which suggests that the micropegs could be exploited to minimize fibrosis and scar formation. Here, we demonstrate that this effect relies on altered adhesive and micromechanical interactions between individual cells and micropegs. First, we show that the proliferation of a cell physically attached to a micropeg is significantly lower than that of a cell cultured on a featureless region of the substrate. Micropeg adhesion is accompanied by a marked elongation in cell and nuclear shape. When fibroblast contractility is pharmacologically attenuated through low-dose inhibition of either Rho-associated kinase or myosin light chain kinase, the potency with which micropeg adhesion suppresses cell proliferation is significantly reduced. Together, our results support a model in which cell fate decisions may be directly manipulated within tissue engineering scaffolds by the inclusion of microtopographical structures that alter cellular mechanics.

Keywords:
- biomaterials
- cell adhesion
- microfabrication
- tissue engineering
- topographical structures

[*] R. G. Thakar, Prof. T. A. Desai
Department of Physiology and
Department of Bioengineering and Therapeutic Sciences
University of California, San Francisco
203C Byers Hall Box 2520, 1700 4th Street
San Francisco, CA 94158-2330 (USA)
Fax: (+1) 415-514-4503
E-mail: tejal.desai@ucsf.edu
M. G. Chown, A. Patel, Prof. S. Kumar
Department of Bioengineering
University of California, Berkeley
274A Stanley Hall #1762
Berkeley, CA 94720-1762 (USA)
Fax: (+1) 510-642-5835
E-mail: skumar@berkeley.edu
A. Patel, L. Peng, Prof. S. Kumar, Prof. T. A. Desai
UCSF/UC Berkeley Joint Graduate Group in Bioengineering

1. Introduction

One of the central challenges of tissue engineering is the design of material scaffolds that offer microscale, cell-specific behavioral cues that vary in precise and predictable ways in space. By providing these cues, one may potentially pattern complex admixtures of cells into functional tissues and organs, as well as promote the physiological activity of one cell type while simultaneously suppressing that of another. Although this task is often accomplished in organismal development through the establishment of complex spatial and temporal gradients of soluble growth, death, and differentiation factors, this approach is not appropriate for tissue engineering and regenerative medicine applications, in which there is often

NANO MICRO small

little direct control over the local soluble milieu of the constituent cells. Instead, over the past two decades, the field has increasingly turned to the engineering of biophysical cues within the underlying material scaffold for this microscale, cell-specific instruction. Indeed, it has been demonstrated that cell growth, death, differentiation, and motility may all be controlled by culturing cells on two-dimensional extracellular matrix (ECM) scaffolds of defined geometry[1–6] and mechanical rigidity.[7–11] Integration of three-dimensional microstructures (microtopographies) into these scaffolds represents a third and comparatively understudied biophysical signal that can strongly influence cell behavior. For example, when vascular smooth muscle cells are cultured on polymeric scaffolds with micrometer-sized grooves, the cells align and elongate within the grooves and undergo concomitant changes in cell morphology and cytoskeletal architecture.[12] Strikingly, when this experiment is repeated with mesenchymal stem cells and the scaffold is subjected to cyclic stretching forces, the cells preferentially differentiate into vascular lineages.[13]

This issue is particularly important in the context of myocardial tissue engineering, in which one must simultaneously create an environment that promotes productive cardiomyocyte function while at the same time limiting the function of cells that promote scar formation. With respect to the former goal, cardiomyocytes, or their cellular progenitors, must be provided with adhesive substrates that enable optimal attachment and alignment, since both of these are needed for coordinated, tissue-scale transmission of electrical signals and contractile forces.[14,15] With respect to the latter issue, endothelial damage associated with either the underlying pathology or introduction of the implant can trigger rampant inflammation,[16,17] ultimately culminating in fibroblast proliferation and activation and the formation of scar tissue.[18,19] In both cases, knowledge of the cellular adhesive and mechanotransductive events that underlie cell–scaffold communication may provide an additional handle for the rational design of tissue engineering scaffolds. For example, it may be possible to incorporate drugs or inhibitory DNA/RNA molecules that reinforce the biophysical cues, much in the spirit of drug- and antisense DNA-eluting vascular stents.[20]

Previously, Russell, Desai, and co-workers developed a microscale tissue engineering scaffold where cells are cultured on microfabricated, polymeric surfaces that contain an array of micrometer-sized protrusions (''micropegs''). These micropegs facilitate cardiomyocyte adhesion and contractility generation; for example, cardiomyocytes cultured on micropeg surfaces readily form adhesions with the micropegs and develop significantly larger myofibrillar masses and more elongated morphologies than cardiomyocytes cultured on flat substrates.[21] When these experiments are repeated with cells capable of undergoing cell division, such as the fibroblasts that accompany the cardiomyocytes in cell isolation, surprising results begin to emerge. In particular, populations of fibroblasts cultured on micropeg surfaces proliferate less rapidly than those cultured on flat surfaces and express lower levels of markers associated with entry into the cell cycle, including cyclin D1.

Interestingly, fibroblast attachment to the micropegs may be attenuated by pharmacological inhibition of Rho-associated kinase (ROCK), which suggests a functional connection between adhesion, contractility, and cell proliferation mediated by the micropegs.[22] These studies have left several unanswered questions about the role of the micropegs in driving cell fate decisions. For example, since these emphasized whole populations of cells, it remains uncertain whether a specific cell attached to a micropeg is any more or less likely to proliferate than its counterpart on a flat portion of the substrate. An alternative possibility would be that cells attached to micropegs participate in cell–cell signaling events that curb proliferation throughout the culture. Moreover, while these studies suggest that micropeg attachment suppresses proliferation by altering the contractile phenotype of the cells, this mechanism has not been directly explored.

Thus, we sought to directly test whether microtopographical cues from the ECM are capable of influencing cell adhesion and proliferation through a mechanobiological mechanism. We cultured fibroblasts and skeletal myoblasts on polymeric micropeg scaffolds and determined if adhesion of a single cell to a single micropeg influenced the likelihood of cell proliferation. We then asked whether this effect depends on the ability of the cell to generate contractile forces through ROCK- and myosin light chain kinase (MLCK)-dependent pathways. Indeed, our studies reveal that micropeg adhesion strongly inhibits cell proliferation at the level of individual cells and micropegs, and that this effect is decreased when the cells' ability to adhere and stress the micropegs is inhibited.

2. Results

2.1. Design of Array

To study the effect of microtopography on cell behavior, we fabricated an array of microscale protrusions (micropegs) out of polydimethylsiloxane (PDMS)[23] (Figure 1A,B). The array dimensions were selected to enable some cells to interact with a single micropeg, some to interact with multiple micropegs, and others to lie entirely within the flat regions between the micropegs. Indeed, when the array was oxidized and passively coated with laminin, thereby rendering it suitable for cell adhesion, we observed all three modes of cell–micropeg interaction (Figure 1C). Scanning electron microscopy (SEM) imaging of the array revealed that the micropegs provide a three-dimensional surface for attachment, and that the cells are capable of interacting with the entire height of a 15-μm-tall peg (Figure 1D). This finding was confirmed by three-dimensional reconstructions of confocal sections (not shown); for example, cells presented with a 15-μm-tall peg ''climb'' the peg to heights ranging from <1 to >10 μm.

2.2. Microposts Alter Cell Proliferation

Previously, we had shown that neonatal rat ventricular fibroblast (NRVF) proliferation decreased when cultured on a micropeg array (10-μm-high pegs in a rectangular pattern with 30- and 100-μm center–center spacing between them).[22] To verify that this effect holds for a fibroblast cell line, we cultured NIH 3T3 fibroblasts on arrays of varying height and spacing.

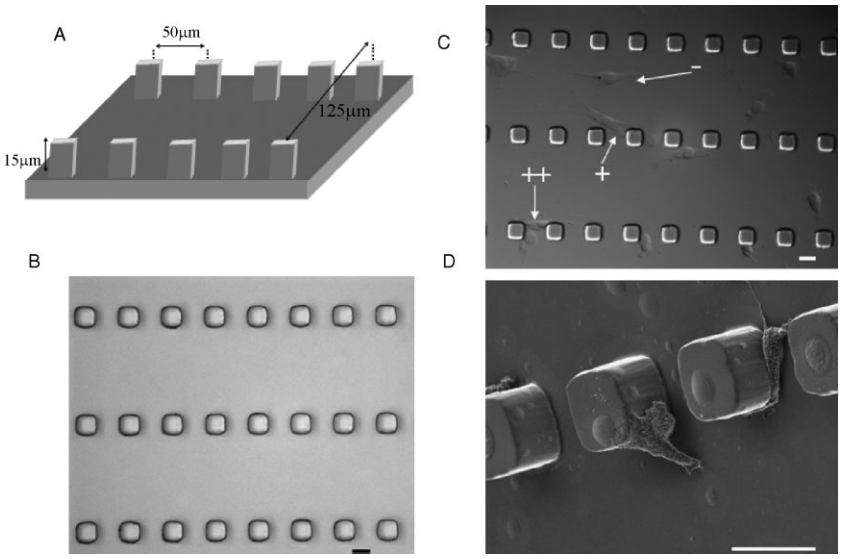

Figure 1. Micropeg arrays for cell adhesion. A) Schematic of the three-dimensional micropeg array. B) Phase-contrast image of the micropegs. C) Phase-contrast image of fibroblasts associated with the micropegs; "+" indicates a cell contacting a micropeg, "++" a cell touching two micropegs, and "−" a cell not contacting a micropeg. D) SEM image of NIH 3T3 fibroblasts interacting with 15-μm-tall micropegs. One cell tethers itself to the substrate and reaches for the top of the micropeg. On the adjacent micropeg, another cell attaches to the base of the micropeg. Scale bar: 25 μm.

with respect to modulating the cells' proliferation. No significant difference existed between the proliferation of fibroblasts in contact with a 5-μm-tall peg versus a 15-μm-tall peg, which suggests that the effect was not enhanced by providing additional contact area for cell adhesion. As expected, increasing the micropeg array spacing to 500 μm, at which very few cells would be expected to contact micropegs, rendered proliferation indistinguishable from that of the nontextured substrate.

To investigate whether the decrease in proliferation was tied to contact with a micropeg, we asked if a correlation existed between a single cell's adhesion to a micropeg and its propensity to proliferate (Figure 3). Cells in direct contact with a micropeg exhibited significantly lower proliferation than their counterparts with no contact to a micropeg or those cultured on a nontextured substrate. These results were also consistent for C2C12 mouse skeletal myoblasts, which indicates that this phenomenon is present in two cell types with different basal levels of contractility and rates of proliferation.

We hypothesized that the presence of the micropeg elicits phenotypic changes, whereas increasing the spacing of the array would lead to no discernible changes. After 24 hours of culture, the micropegs significantly decreased fibroblast proliferation (Figure 2). Micropeg height did not play a role

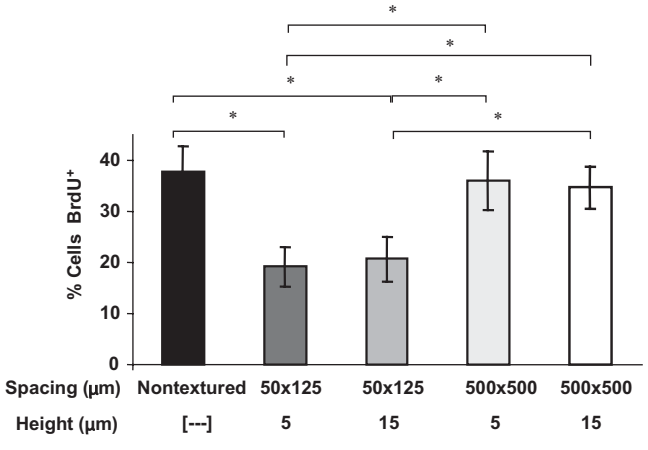

Figure 2. Micropegs affect fibroblast proliferation. Fibroblasts were seeded onto four micropeg arrays ($50 \times 125 \times 5$, $50 \times 125 \times 15$, $500 \times 500 \times 5$, $500 \times 500 \times 15$ μm) and a nontextured control surface. Proliferation fell dramatically (* denotes $p < 0.001$) on substrates bearing 5- or 15-μm-tall micropegs spaced at a center-to-center distance of 50×125 μm (in each direction) compared to either nontextured control substrates or substrates in which the micropegs were spaced at a center-to-center distance of 500×500 μm. Results are representative of at least three independent experiments. BrdU = 5-bromo-2′-deoxyuridine.

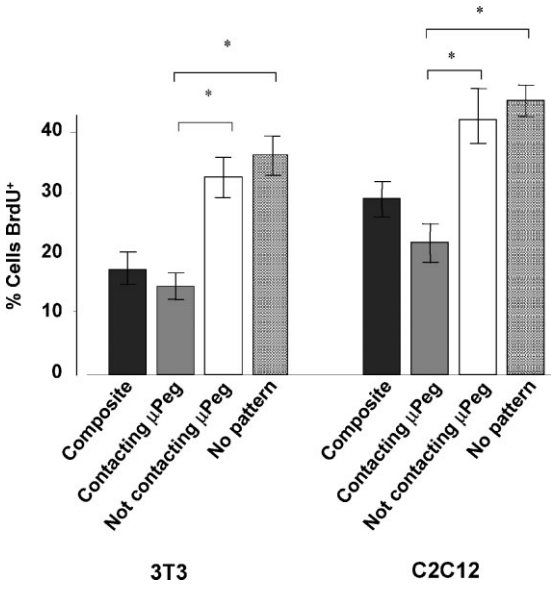

Figure 3. Proliferation effects are dependent upon cell–micropeg interactions. In both 3T3 fibroblasts and C2C12 skeletal myoblasts, proliferation decreased (* denotes $p < 0.01$) in cells making direct contact with a micropeg (μPeg), whereas cells not in contact with a micropeg exhibited proliferation rates similar to cells cultured on control, nontextured surfaces. The term "composite" refers to measurements taken on micropeg-textured surfaces, but without regard to whether a particular cell is or is not contacting a micropeg. It therefore includes contributions from both the "contacting μPeg" and "not contacting μPeg" categories.

small NANO MICRO

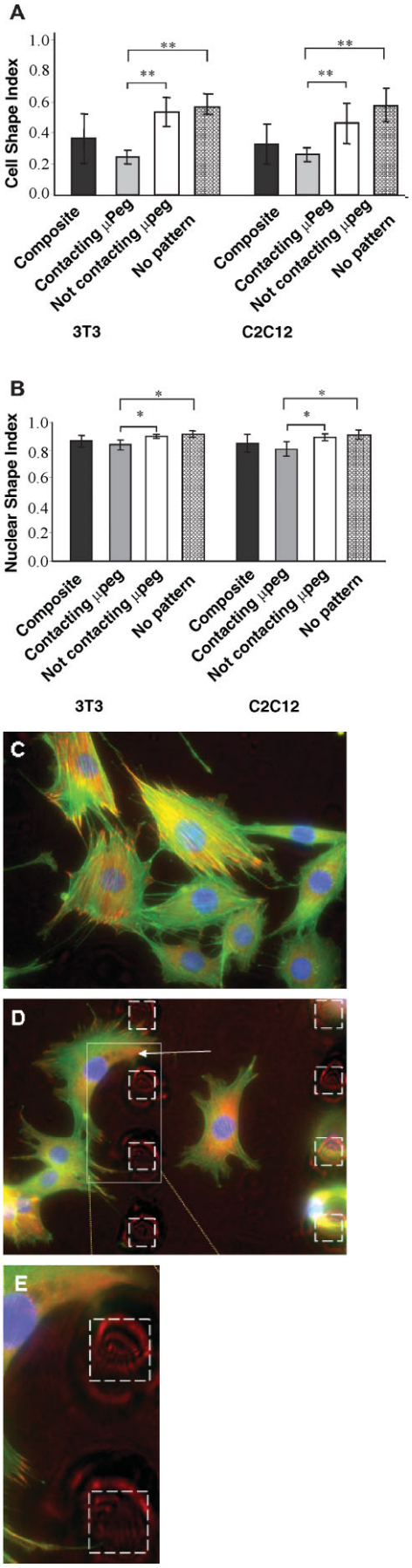

2.3. Link of Cell Proliferation to Cell and Nuclear Shape, Cytoskeletal Organization, and Focal Adhesion Formation

Changes in proliferation are often accompanied by changes in cell and nuclear morphology, which in turn are indicators of changes in gene program and cellular contractility.[24,25] In our system, cells in contact with a micropeg were more significantly elongated than cells not in contact with a micropeg or those cultured on a nontextured substrate. There were significant differences in the cell shape index (CSI) of the fibroblasts and skeletal myoblasts (Figure 4A). In both cases, cells in contact with a micropeg had a significantly lower CSI than those not in direct contact with a micropeg. Changes in the cell shape correlated with alteration in nuclear shape, as quantified by the nuclear shape index (NSI; Figure 4B). There was again a distinct divide between nuclear shape in cells in contact with a micropeg and in cells not in contact with a micropeg, regardless of cell type. We next examined whether micropegs were capable of supporting physiologically functional adhesion complexes. Fibroblasts formed vinculin-containing focal adhesions in close vicinity to the micropegs (Figure 4C–E).

2.4. Influence of Micropegs is Partially Suppressed by Inhibition of ROCK or MLCK

Based on the observed changes in cell shape and cytoskeletal organization induced by micropeg adhesion, we hypothesized that the attendant suppression of proliferation is tied to changes in cellular contractility. To test this directly, we pharmacologically inhibited two key cellular enzymes that regulate myosin-dependent contractility: ROCK and MLCK.[26–28] When fibroblasts were cultured in the presence of the ROCK inhibitor Y27632, the micropegs continued to suppress proliferation on cells in direct contact with micropegs to the same extent as the nondrug controls (Figure 5A). Similarly, micropeg adhesion suppressed proliferation for cells cultured in the presence of the MLCK inhibitor ML7, despite the fact that overall proliferation increased slightly. When data from these experiments are represented ratiometrically, it becomes clear that inhibition of either ROCK or MLCK partially reverses the ability of the micropegs to suppress proliferation ($p < 0.05$ in both cases; Figure 5B). Importantly, and as expected, differences in proliferation between completely flat substrates (''no pattern'') and flat regions of patterned substrates (''not contacting μPeg'') were not statistically significant ($p > 0.05$) for any of the conditions studied.

Figure 4. Cell and nuclear shape indices correlate with proliferation on micropegs. A) 3T3 and C2C12 cells in contact with a micropeg had lower CSIs, and therefore a more linear morphology than their counterparts not in contact with a micropeg B) Similarly, micropeg adhesion significantly influenced nuclear morphology, as the NSI fell when cells were in contact with a micropeg (* denotes $p < 0.05$ and ** denotes $p < 0.005$). C) 3T3 fibroblasts stained for nuclear DNA (blue), F-actin (green), and vinculin (red) are shown on a nontextured substrate. D) Fibroblasts cultured on textured substrates extended processes that form adhesions with the micropegs. E) A higher-magnification view of the vinculin staining around two micropegs. The white dashed squares are 25×25 μm and represent the positions of the micropegs.

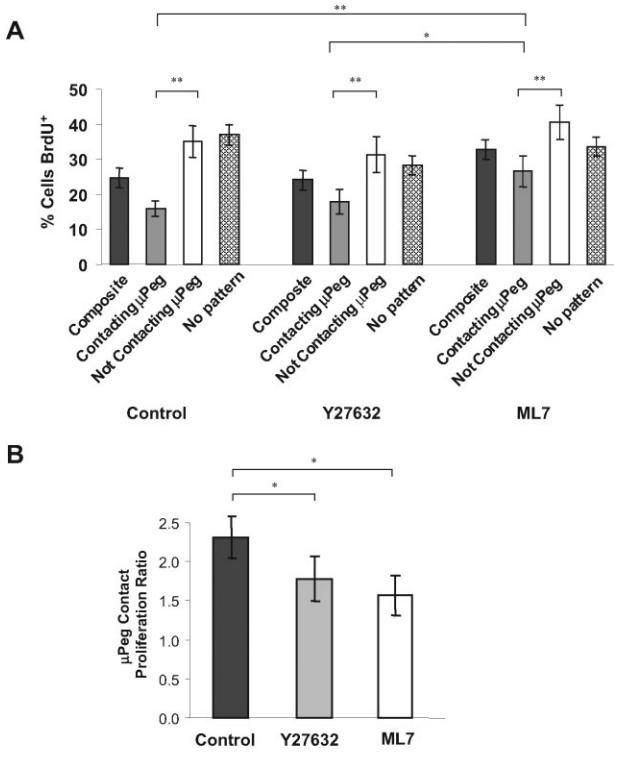

Figure 5. Contractile inhibitors suppress the function of micropegs. A) The addition of either Y27632 or ML7 to the culture reduces proliferation in cells attached to a micropeg. B) The μPeg contact proliferation ratio represents the ratio of the percentage of $BrdU^+$ cells not touching a micropeg to the percentage of $BrdU^+$ cells in contact with a micropeg under each condition. The results represent three independent experiments, with each yielding three to four viewing fields (* denotes $p < 0.05$ and ** denotes $p < 0.005$).

2.5. Microposts Provide Support and Partially Suppress Contractile Inhibitor Function

To rule out the possibility that the contractility inhibitors could be exerting their effects by reducing cell adhesion to the micropegs, we quantified the number of micropegs engaged by each cell under each drug treatment (Figure 6A). Surprisingly, we found that inhibition of either ROCK or MLCK increased the likelihood of individual cells adhering to micropegs. Subsequent imaging revealed that contractility-inhibited cells cultured on nontextured substrates displayed a characteristic loss of stress fibers and reduced cell spreading (Figure 6B).

3. Discussion

We have shown that adhesion of cultured cells to microscale protrusions is sufficient to induce specific alterations in cell physiology that include cell and nuclear elongation, reorganization of cytoskeletal and adhesive structures, and, most strikingly, reduced cell proliferation. We have also shown that these effects depend on MLCK- and ROCK-dependent contractility, as pharmacological inhibition of these enzymes decreases the ability of the micropegs to induce these changes. This suggests a mechanism where cell–micropeg adhesion facilitates the generation of contractile forces, which in turn activates a broader gene program that influences morphology, cytoskeletal architecture, and ultimately cell fate (Figure 7). Our findings add additional support to the broadly emerging notion that mechanical inputs to cells can profoundly influence canonical cell behaviors through actomyosin-based signaling events.[29–31]

It is important to note that we found adhesion-dependent suppression of proliferation in two physiologically distinct cell lines: NIH 3T3 fibroblasts and C2C12 skeletal myoblasts. Even in the undifferentiated (i.e., nonsyncytiated) state, C2C12 myoblasts display highly developed and aligned contractile myofibrils on completely flat substrates;[32] moreover, C2C12 myoblasts proliferate at a much higher basal rate than NIH 3T3 fibroblasts.[33–35] Thus, it is remarkable that micropeg adhesion alone is capable of stunting C2C12 proliferation to such a significant degree. This finding also suggests that micropegs may be incorporated into tissue engineering scaffolds as a generalizable strategy for controlling proliferation, even in cell types that proliferate at prodigious rates or do not require topographical cues to develop an oriented cytoskeleton or exert significant contractile forces. In exploring the mechanism of the micropegs' ability to curb proliferation, we inhibited cellular contractility through two nominally independent mechanisms: ROCK and MLCK. Intriguingly, both ROCK and MLCK inhibition reduced the ability of micropeg adhesion to suppress proliferation, even though each enzyme activates a distinct pool of cellular myosins.[36,37] We also observed that inhibition of either ROCK or MLCK increased micropeg adhesion; it is unclear why this is the case, but to a first approximation one can envision two alternative possibilities: first, inhibition of contractility could cause the cells to ''seek out'' micropegs, possibly for mechanical support; second, inhibition of contractility could render the cells unable to fully dissociate from the micropegs once adhesions are formed. High-resolution time-lapse imaging of cells migrating on these scaffolds would help distinguish between these two hypotheses.

While our studies provide a clear phenomenological link between cell contractility and proliferation, the precise mechanism remains unclear. Indeed, our results raise the question of whether adhesive contacts formed against the vertically oriented micropegs are fundamentally different from adhesive contacts formed on flat portions of the substrate, and if so, how these differences give rise to the observed changes in physiology. The finding that suppression of proliferation is independent of micropeg height suggests that these effects are not due strictly to altered numbers of integrin–ECM contacts. One possibility is that the micropegs alter the distribution or mean area of cell–ECM focal adhesions, consistent with previous studies that demonstrate that focal adhesion size correlates with generation of cell–ECM traction and traction-dependent behaviors.[38–40] Another possibility is that attachment to a vertically oriented surface provides a geometry that favors optimal anchoring of cellular contractile elements, such as stress fibers.[41] This notion is supported by earlier studies, which demonstrated

small NANO MICRO

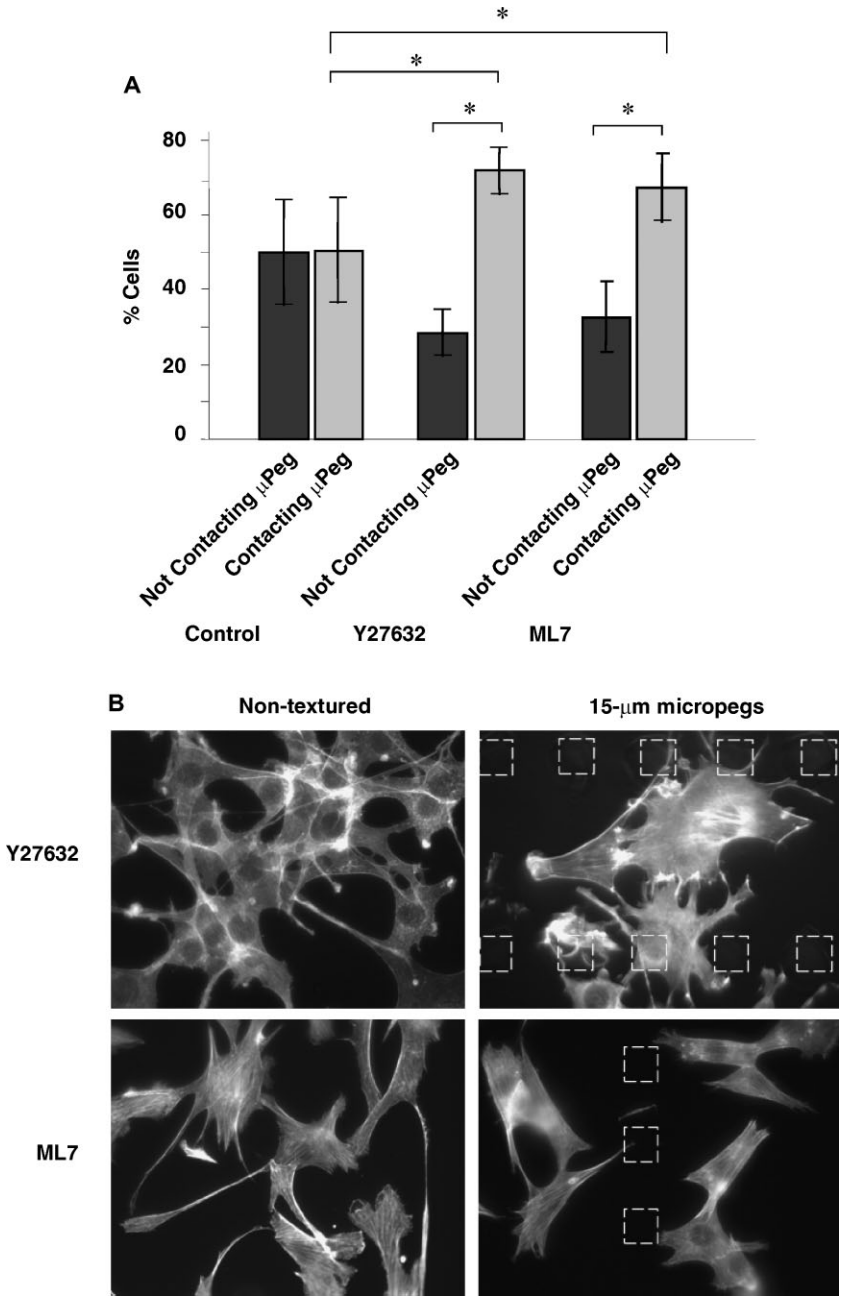

Figure 6. Fibroblasts increase adhesion to micropegs with administration of contractile inhibitors. A) The addition of Y27 and ML7 at 25 μM increases the tendency of 3T3 fibroblasts to adhere to micropegs (* denotes $p < 0.001$) Results are representative of five independent experiments yielding three to four viewing fields per experiment. B) Fluorescence imaging of F-actin reveals that inhibition of contractility produces characteristic changes in cell morphology and micropeg adhesion. The white dotted square is 25 × 25 μm and represents the position of the micropeg.

significant increases in myofibrillar mass in cardiomyocytes attached to micropegs.[22] Direct comparison of the contractility of cells attached to micropegs with that of cells cultured on flat substrates would help to explore this hypothesis more fully. Another possibility is that micropeg-bound adhesions contain different panels of adhesive proteins than their counterparts on flat substrates. Although we find that both populations of adhesions are vinculin-positive, this does not rule out the possibility that the distributions of other adhesive proteins may differ, particularly those that participate in the sensing of mechanical inputs from the ECM.[42]

Micropeg adhesion gives rise to a pronounced elongation of cell and nuclear morphology. Changes in both of these parameters have been associated with altered cell fate decisions in many systems in which cells are cultured on engineered scaffolds. For example, endothelial cells proliferate when allowed to spread onto large ECMs but apoptose when restricted to comparatively small ECMs.[1] Cell shape has also been shown to guide developmental trajectories in mesenchymal stem cells in a manner that is largely independent of soluble factors.[43] Similarly, nuclear shape has been correlated in several cell types with cell proliferation and differentiation[44,45] and secretion of ECM components.[46] Nuclear shape has also been shown to influence the rate of transport through to the nucleus and affect the size and confirmation of nuclear pores and the genetic material inside the nucleus.[47] In considering the mechanistic link between micropeg adhesion and proliferation, many studies have revealed direct physical connections between cell-surface integrins and cell and nuclear architecture,[48–51] which suggests strongly that the cytoskeleton is the physical actuator that translates forces applied at the cell surface into shape-dependent physiology. This is manifested in our experiments by the finding that cell–micropeg adhesion and adhesion-dependent suppression are profoundly affected when cell contractility is pharmacologically inhibited. Given this likely connection of integrin engagement to the cytoskeleton, it would be interesting to determine if the phenomena we observe depend on ligation of specific integrin subtypes or on the integrity of other cytoskeletal networks (microtubules, intermediate filaments).

Returning to the broader question of achieving microscale and spatially variable control of cell function in tissue engineering systems, our studies illustrate how relatively simple microscale topographical cues can be exploited to control proliferation rates from region to region in a single culture. It is conceivable that the adhesion-dependent proliferation observed here holds to varying degrees in different cell types, and in some cases may even follow an inverse relationship in which micropeg attachment promotes cell division. If this is the case, scaffolds like those used here could be designed with complex topographic patterns that selectively trigger changes

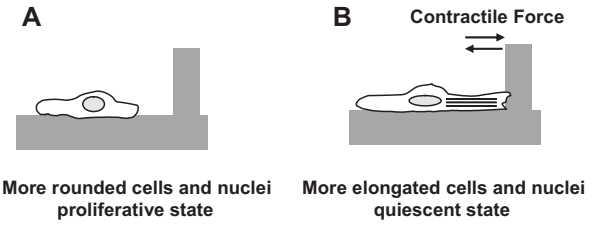

Figure 7. A model for micropeg-induced changes in cell morphology and contractility. A) A cell is depicted not to be in contact with a micropeg. This situation results in a lower CSI, NSI, and normal proliferation from the cell. B) A cell is shown in contact with a micropeg. The contact yields a quiescent cell with a lower CSI and NSI.

in cell morphology, mechanics, and division at specific portions of the substrate, which could in turn provide the basis for guided assembly of complex, multicellular tissues. This prospect is particularly exciting given the recent explosion of work demonstrating that microscale, biophysical cues can direct stem cells down different developmental lineages.[13,43,52,53] Additionally, it would be interesting to determine whether and to what extent these microtopographical cues can be combined with more traditional biochemical signals that are either immobilized on the scaffold (e.g., ECM-mimetic peptides) or released from the scaffold (e.g., eluted growth factors). Finally, there may even be an opportunity to combine scaffolds like these with active imposition of mechanical force on the microscale,[54] thus offering a route to control cell–scaffold mechanobiological crosstalk in the context of microscale actuators and devices.

4. Conclusions

We have shown that adhesion of cultured fibroblasts and myoblasts to microscale topographical cues leads to decreased cell proliferation, which is in turn dependent on the cells' ability to generate contractile force. Our finding adds new support to the notion that adhesion, contractility, and proliferation are intimately connected, and suggests that these connections can be exploited to control cell behavior in microengineered scaffolds for tissue engineering and regenerative medicine.

5. Experimental Section

Fabrication of micropeg arrays: Micropeg arrays were fabricated as reported previously.[21,22,55] To construct a photoresist (PR) mold, SU-8 2010 negative PR (Microchem, Newton, MA, USA) was spin-coated onto a single-crystal silicon wafer to a thickness of either 5 or 15 μm and baked at 95 °C for 3 min. Microscale holes were introduced by placing a patterned photomask over the coated wafer and exposing it to UV light for 25–30 s at an intensity of 5 mW cm^{-2}. The uncrosslinked PR was then removed by washing the wafer in SU-8 developer (Microchem) for 30 s, and then the SU-8 molds were baked at 95 °C for 3 min. The dimensions of the resulting microscale holes were then verified by light microscopy and surface profilometry. To create polymeric micropeg arrays for cell culture, PDMS and curing agent were prepared and mixed as directed by the manufacturer (Sylgard 184, Dow Corning, MI), degassed under vacuum, poured onto the SU-8 mold, and spin-coated at 200 rpm for 1 min followed by 250 rpm for 30 s to achieve a thickness of 5 or 15 μm. The PDMS–wafer composite was then baked for >2 h at 70 °C. After the PDMS had cured, the micropatterned PDMS membranes were peeled from the SU-8 masters. Unpatterned PDMS membranes were fabricated in an identical manner, except for the use of unpatterned, non-PR-coated silicon wafers as masters. Prior to use in cell culture experiments, the PDMS was rendered hydrophilic by exposure to oxygen plasma and then incubated with mouse laminin (Invitrogen, Carlsbad, CA) at a concentration of 0.05 mg mL^{-1} in phosphate-buffered saline (pH 7.4) for 60 min at 4 °C.

Cell culture: NIH 3T3 mouse fibroblasts and C2C12 mouse myoblasts (ATCC, Manassas, VA) were cultured on tissue culture plastic in a complete medium consisting of Dulbecco's Modified Eagle's Medium (DMEM) with 10% fetal bovine serum and 1% penicillin/streptomycin (Gibco-BRL, Grand Island, NY). Cell cultures were maintained in a humidity-controlled 5% CO_2 incubator at 37 °C. Prior to seeding on fabricated substrates, cells were allowed to grow to about 90% confluence, trypsinized, resuspended in complete medium, plated on the fabricated surfaces at a density of 10 000 cells cm^{-2}, and washed after 10–20 min to remove nonadherent cells. Longer incubation times led to an overly confluent substrate, and lower seeding densities at higher incubation times failed to produce a sufficient density of cells on the micropeg-bearing portion of the substrate for statistical analysis.

SEM: Cells were fixed in a 3% glutaraldehyde (Sigma–Aldrich, St. Louis, MO) in 0.1 M sucrose-cacodylate (Sigma–Aldrich, St. Louis, MO) buffer for 72 h at room temperature. Following fixation, samples were rinsed three times in 0.1 M sucrose-cacodylate buffer for 5 min. Samples were then dehydrated by removing the buffer and adding and replacing a series of ethanol solutions in a graded series as follows: 35, 50, 70, 95, and 100% (twice). Each ethanol solution was applied for 10 min. The final 100% ethanol solution was replaced with hexamethyldisilazane (HMDS; Polysciences, Inc., Warrington, PA) for 10 min and removed promptly. Samples were allowed to air dry for 30 min and then sputter-coated with a gold–palladium alloy.

Immunofluorescence staining: Cells were fixed in 4% paraformaldehyde (Fisher Scientific, Pittsburgh, PA) for 15 min, permeabilized with 0.5% Triton X-100 (Sigma, St. Louis, MO) for 15 min, and blocked with 1% bovine serum albumin (BSA; Sigma, St. Louis, MO) for 30 min. F-actin was stained using Alexa Fluor 488 phalloidin (Molecular Probes, Eugene, OR) for 30 min. To stain for vinculin, following the blocking step, cells were incubated with mouse anti-vinculin IgG (Sigma, St. Louis, MO) for 1.5 h at room temperature, and incubated with Alexa 563-conjugated donkey anti-mouse IgG (Molecular Probes, Eugene, OR) for 1 h at room temperature. Nuclei were stained with Hoechst 33258 (Molecular Probes, Eugene, OR). All images were acquired on a Nikon TE3000U epifluorescence microscope.

Measurement of cell proliferation: Cell proliferation was measured by incorporation of 5-bromo-2′-deoxyuridine (BrdU).

NANO MICRO small

Cells were cultured in complete medium for 24 h, incubated with 10 μM BrdU (Amersham, Piscataway, NJ) for 1 h, and then fixed with paraformaldehyde. To determine the incorporation of BrdU, cells were pretreated with 50% methanol, permeabilized with 0.5% Triton X-100, and then treated with 2N HCl. BrdU was stained by treating the cells with a mouse anti-BrdU primary antibody (BD Biosciences, San Jose, CA) and a fluorescein isothiocyanate-tagged goat-anti-mouse secondary antibody (Jackson ImmunoResearch). Cell nuclei were stained with 1 μg mL^{-1} propidium iodide (PI; Molecular Probes) for 5 min. The percentage of BrdU-positive nuclei was determined by dividing the number of BrdU-positive nuclei (defined by co-incorporation of BrdU and PI) by the total number of nuclei (defined by incorporation of PI).

Contractility inhibitors: To abrogate cellular contractility, Y-27632 was used to inhibit ROCK and ML-7 was used to inhibit MLCK (Calbiochem, San Diego, CA). Both drugs were diluted to 25 μM in complete medium prior to addition to the cultures. In all cases, cells were seeded and allowed to attach and spread for 2 h before application of the drug, and the drug was left in the culture for 24 h prior to analysis.

Morphometric analysis: CSI was defined here as the dimensionless ratio 4π(cell area) (cell perimeter)$^{-2}$. CSI is a measure of the circularity of a cell; circular-shaped cells have CSI values approaching 1, and elongated cells have CSI values approaching 0. Similarly, the NSI was defined as 4π(nuclear area) (nuclear perimeter)$^{-2}$. Both CSI and NSI were determined directly from phase-contrast images.

Statistical analysis: Statistically significant differences in multicondition data sets were detected by performing analysis of variance (ANOVA). Sequential Holm *t*-tests were then performed to identify differences between specific pairs of conditions.

Acknowledgements

We appreciate Dr. Kurt Thorn's invaluable training and assistance at the Nikon Imaging Center at UCSF–Mission Bay. In addition, we would like to express our thanks to Dr. Daniel A. Bernards for his help with SEM image collection. We also thank the UCSF Biomedical Micro- and Nanofabrication Core for allowing us to fabricate our SU-8 molds, and Dr. James J. Norman and Mark Steedman for guidance with the fabrication. This research was supported by an NSF NSEC grant to T.A.D., an American Heart Association Beginning Grant-in-Aid (0765128Y) and Arnold and Mabel Beckman Young Investigator Award to S.K., and a UCSF Dean's Health Science Fellowship to L.P. All SEM was performed at the Stanford Nanocharacterization Laboratory through the Stanford CIS grant program.

[1] C. S. Chen, M. Mrksich, S. Huang, G. M. Whitesides, D. E. Ingber, *Science* **1997**, *276*, 1425–1428.
[2] Y. C. Wang, C. C. Ho, *FASEB J.* **2004**, *18*, 525–527.
[3] R. S. Kane, S. Takayama, E. Ostuni, D. E. Ingber, G. M. Whitesides, *Biomaterials* **1999**, *20*, 2363–2376.
[4] C. J. Lee, M. S. Blumenkranz, H. A. Fishman, S. F. Bent, *Langmuir* **2004**, *20*, 4155–4161.
[5] H. Huang, R. D. Kamm, R. T. Lee, *Am. J. Physiol. Cell Physiol.* **2004**, *287*, C1–C11.
[6] K. R. Milner, C. A. Siedlecki, *J. Biomed. Mater. Res. A* **2007**, *82*, 80–91.
[7] J. A. Pedersen, M. A. Swartz, *Ann. Biomed. Eng.* **2005**, *33*, 1469–1490.
[8] A. J. Engler, S. Sen, H. L. Sweeney, D. E. Discher, *Cell* **2006**, *126*, 677–689.
[9] A. Saez, M. Ghibaudo, A. Buguin, P. Silberzan, B. Ladoux, *Proc. Natl. Acad. Sci. USA* **2007**, *104*, 8281–8286.
[10] C. S. Wallace, S. A. Strike, G. A. Truskey, *Am. J. Physiol. Heart Circ. Physiol.* **2007**, *3*, 1978–1986.
[11] J. Salber, S. Grater, M. Harwardt, M. Hofmann, D. Klee, J. Dujic, H. Jinghuan, J. Ding, S. Kippenberger, A. Bernd, J. Groll, J. P. Spatz, M. Moller, *Small* **2007**, *3*, 1023–1031.
[12] R. G. Thakar, F. Ho, N. F. Huang, D. Liepmann, S. Li, *Biochem. Biophys. Res. Commun.* **2003**, *307*, 883–890.
[13] K. Kurpinski, J. Chu, C. Hashi, S. Li, *Proc. Natl. Acad. Sci. USA* **2006**, *103*, 16095–16100.
[14] R. K. Birla, G. H. Borschel, R. G. Dennis, *Artif. Organs* **2005**, *29*, 866–875.
[15] J. Leor, S. Aboulafia-Etzion, A. Dar, L. Shapiro, I. M. Barbash, A. Battler, Y. Granot, S. Cohen, *Circulation* **2000**, *102*, III56–III61.
[16] G. M. Puddu, E. Cravero, G. Arnone, A. Muscari, P. Puddu, *J. Biomed. Sci.* **2005**, *12*, 839–853.
[17] A. B. Reiss, A. D. Glass, *J. Investig. Med.* **2006**, *54*, 123–131.
[18] G. Ren, O. Dewald, N. G. Frangogiannis, *Curr. Drug Targets Inflamm. Allergy* **2003**, *2*, 242–256.
[19] Y. Sun, M. F. Kiani, A. E. Postlethwaite, K. T. Weber, *Basic Res. Cardiol.* **2002**, *97*, 343–347.
[20] H. Takahashi, D. Letourneur, D. W. Grainger, *Biomacromolecules* **2007**, *8*, 3281–3293.
[21] D. Motlagh, S. E. Senyo, T. A. Desai, B. Russell, *Biomaterials* **2003**, *24*, 2463–2476.
[22] S. Y. Boateng, T. J. Hartman, N. Ahluwalia, H. Vidula, T. A. Desai, B. Russell, *Am. J. Physiol. Cell Physiol.* **2003**, *285*, C171–C182.
[23] G. M. Whitesides, E. Ostuni, S. Takayama, X. Jiang, D. E. Ingber, *Annu. Rev. Biomed. Eng.* **2001**, *3*, 335–373.
[24] A. Lang, D. A. Brenner, *Ital. J. Gastroenterol. Hepatol.* **1999**, *31*, 173–179.
[25] S. Pelletier, C. Julien, M. R. Popoff, N. Lamarche-Vane, S. Meloche, *J. Cell Physiol.* **2005**, *204*, 412–422.
[26] G. Totsukawa, Y. Yamakita, S. Yamashiro, D. J. Hartshorne, Y. Sasaki, F. Matsumura, *J. Cell Biol.* **2000**, *150*, 797–806.
[27] F. Matsumura, *Trends Cell Biol.* **2005**, *15*, 371–377.
[28] J. A. McKenzie, A. J. Ridley, *J. Cell Physiol.* **2007**, *213*, 221–228.
[29] K. Clark, M. Langeslag, C. G. Figdor, F. N. van Leeuwen, *Trends Cell Biol.* **2007**, *17*, 178–186.
[30] K. Katoh, Y. Kano, M. Amano, H. Onishi, K. Kaibuchi, K. Fujiwara, *J. Cell Biol.* **2001**, *153*, 569–584.
[31] M. Yanase, H. Ikeda, I. Ogata, A. Matsui, E. Noiri, T. Tomiya, M. Arai, Y. Inoue, K. Tejima, K. Nagashima, T. Nishikawa, M. Shibata, M. Ikebe, M. Rojkind, K. Fujiwara, *Biochem. Biophys. Res. Commun.* **2003**, *305*, 223–228.
[32] D. K. McMahon, P. A. Anderson, R. Nassar, J. B. Bunting, Z. Saba, A. E. Oakeley, N. N. Malouf, *Am. J. Physiol.* **1994**, *266*, C1795–C1802.
[33] G. Biswas, H. K. Anandatheerthavarada, N. G. Avadhani, *Cell Death Differ.* **2005**, *12*, 266–278.
[34] R. G. Dennis, P. E. Kosnik, II, M. E. Gilbert, J. A. Faulkner, *Am. J. Physiol. Cell Physiol.* **2001**, *280*, C288–C295.
[35] P. E. Kosnik, J. A. Faulkner, R. G. Dennis, *Tissue Eng.* **2001**, *7*, 573–584.
[36] K. Katoh, Y. Kano, S. Ookawara, *Genes Cells* **2007**, *12*, 623–638.
[37] G. Totsukawa, Y. Wu, Y. Sasaki, D. J. Hartshorne, Y. Yamakita, S. Yamashiro, F. Matsumura, *J. Cell Biol.* **2004**, *164*, 427–439.

[38] J. L. Tan, J. Tien, D. M. Pirone, D. S. Gray, K. Bhadriraju, C. S. Chen, *Proc. Natl. Acad. Sci. USA* **2003**, *100*, 1484–1489.
[39] N. Q. Balaban, U. S. Schwarz, D. Riveline, P. Goichberg, G. Tzur, I. Sabanay, D. Mahalu, S. Safran, A. Bershadsky, L. Addadi, B. Geiger, *Nat. Cell Biol.* **2001**, *3*, 466–472.
[40] J. M. Goffin, P. Pittet, G. Csucs, J. W. Lussi, J. J. Meister, B. Hinz, *J. Cell Biol.* **2006**, *172*, 259–268.
[41] S. Kumar, I. Z. Maxwell, A. Heisterkamp, T. R. Polte, T. P. Lele, M. Salanga, E. Mazur, D. E. Ingber, *Biophys. J.* **2006**, *90*, 3762–3773.
[42] T. P. Lele, J. Pendse, S. Kumar, M. Salanga, J. Karavitis, D. E. Ingber, *J. Cell Physiol.* **2006**, *207*, 187–194.
[43] R. McBeath, D. M. Pirone, C. M. Nelson, K. Bhadriraju, C. S. Chen, *Dev. Cell* **2004**, *6*, 483–495.
[44] D. E. Ingber, D. Prusty, Z. Sun, H. Betensky, N. Wang, *J. Biomech.* **1995**, *28*, 1471–1484.
[45] S. A. Lelievre, M. J. Bissell, P. Pujuguet, *Crit. Rev. Eukaryot. Gene Expr.* **2000**, *10*, 13–20.
[46] C. H. Thomas, J. H. Collier, C. S. Sfeir, K. E. Healy, *Proc. Natl. Acad. Sci. USA* **2002**, *99*, 1972–1977.
[47] C. M. Feldherr, D. Akin, *J. Cell Biol.* **1990**, *111*, 1–8.
[48] A. J. Maniotis, C. S. Chen, D. E. Ingber, *Proc. Natl. Acad. Sci. USA* **1997**, *94*, 849–854.
[49] A. S. Belmont, F. M. Kendall, C. A. Nicolini, *Cell Biophys.* **1980**, *2*, 165–175.
[50] M. J. Dalby, M. O. Riehle, D. S. Sutherland, H. Agheli, A. S. Curtis, *Eur. J. Cell Biol.* **2004**, *83*, 159–169.
[51] S. Hu, J. Chen, N. Wang, *Front. Biosci.* **2004**, *9*, 2177–2182.
[52] A. Chaubey, K. J. Ross, R. M. Leadbetter, K. J. Burg, *J. Biomed. Mater. Res. B. Appl. Biomater.* **2008**, *84*, 70–78.
[53] R. Peerani, B. M. Rao, C. Bauwens, T. Yin, G. A. Wood, A. Nagy, E. Kumacheva, P. W. Zandstra, *EMBO J.* **2007**, *26*, 4744–4755.
[54] N. J. Sniadecki, A. Anguelouch, M. T. Yang, C. M. Lamb, Z. Liu, S. B. Kirschner, Y. Liu, D. H. Reich, C. S. Chen, *Proc. Natl. Acad. Sci. USA* **2007**, *104*, 14553–14558.
[55] J. Deutsch, D. Motlagh, B. Russell, T. A. Desai, *J. Biomed. Mater. Res.* **2000**, *53*, 267–275.

Received: December 22, 2007
Revised: May 21, 2008

